ACCSCIENCE PUBLISHING

Journal of Energy and Sustainability

ORIGINAL RESEARCH ARTICLE

Sustainable amorphous porous carbon for efficient removal of industrial dyes

Dayane G. Domingos[1]*, Beatriz Lima Santos Klienchen Dalari[2], Marina C. de Moraes[1], Antonio I. Ramos Filho[3], Luís A. M. Ruotolo[4], Maria Ángeles Lobo-Recio[1], and Maria Eliza Nagel-Hassemer[1]

[1]Department of Environmental Engineering, Center of Technological Sciences (CTC), Federal University of Santa Catarina (UFSC), Florianópolis, Santa Catarina, Brazil

[2]Department of Environmental and Sanitary Engineering, School of Engineering and Applied Sciences, University of Vale do Itajaí (UNIVALI), Itajaí, Santa Catarina, Brazil

[3]Department of Materials Engineering, Center of Technological Sciences (CTC), Federal University of Santa Catarina (UFSC), Florianópolis, Santa Catarina, Brazil

[4]Department of Chemical Engineering, Center for Exact Sciences and Technology (CCET), Federal University of São Carlos (UFSCar), São Carlos, São Paulo, Brazil

Abstract

Cork, a porous biopolymer, is composed of hollow prismatic cells with thin walls arranged in a compact honeycomb-like structure, making it a promising material for adsorption applications. In this study, cork-derived activated carbon (CAC) was synthesized through pyrolysis followed by chemical activation using solid potassium hydroxide, with the aim of producing an efficient adsorbent for the removal of industrial dyes. The structure, morphology, and functional groups of the CAC were characterized using Brunauer-Emmett-Teller (BET) surface area analysis, scanning electron microscopy, thermogravimetric analysis, Fourier transform infrared spectroscopy, and X-ray diffraction. BET surface area analysis revealed a high specific surface area of 1,793 m^2/g, favoring strong adsorption capacity. Batch and fixed-bed column experiments were conducted to evaluate the adsorption performance toward two representative dyes: Methylene blue (MB) and reactive red (RR). The pseudo-second-order kinetic model accurately described the adsorption behavior, while the Langmuir isotherm model indicated monolayer adsorption for MB, and the Freundlich model better fitted the heterogeneous adsorption of RR. The maximum adsorption capacities (q_m) were 250 mg/g and 105 mg/g for MB and RR, respectively. Overall, the results demonstrate that the produced CAC exhibits high adsorption efficiency and holds significant potential for application in industrial effluent remediation and the treatment of water contaminated with persistent dye compounds.

Keywords: Activated carbon; Adsorption; Cork; Industrial effluents

***Corresponding author:**
Dayane G. Domingos
(dayane.domingos@posgrad.ufsc.br)

Citation: Domingos DG, Dalari BLSK, de Moraes MC, *et al*. Sustainable amorphous porous carbon for efficient removal of industrial dyes. *Journal of Energy and Sustainability*. 2025;1(2):025320016. doi: 10.36922/JES025320016

Received: August 7, 2025

Revised: September 25, 2025

Accepted: October 9, 2025

Published online: October 30, 2025

1. Introduction

Global sustainability has become a central axis in scientific and industrial efforts, driven by the urgent need to mitigate environmental impacts and optimize the use of natural resources.[1-3] Within this context, the reuse of industrial waste stands out as a key strategy

to promote the circular economy and develop sustainable technologies. Among the most relevant waste materials, cork stoppers—by-products of the wine industry—represent a promising resource owing to their low carbon footprint and renewable characteristics.

Cork, derived from the cork oak tree (*Quercus suber*), is widely recognized as a renewable natural material characterized by low density, flexibility, and high resistance to chemical degradation.[4] Despite its economic and environmental relevance, a significant amount of used cork stoppers is not properly treated, resulting in the loss of valuable resources and environmental issues such as waste accumulation in landfills.[5-7] Moreover, direct use of cork stoppers is limited, as their physical and chemical properties deteriorate during use. In this scenario, valorizing cork waste through chemical and thermal transformations emerges as a promising alternative to reduce the environmental impact associated with its disposal.[5,6]

At the same time, the increasing contamination of water bodies by industrial effluents has become a global concern. Among the most persistent pollutants are synthetic dyes, extensively used in the textile, paper, plastic, and leather industries. These organic compounds exhibit high toxicity, chemical stability, and resistance to conventional degradation processes, making their treatment and removal particularly challenging. The presence of these dyes in wastewater not only degrades environmental quality but also poses significant risks to human health and aquatic biodiversity. Therefore, the development of effective and affordable technologies for the treatment of these pollutants has become a priority in the environmental field.[8,9]

In this context, activated carbon produced from lignocellulosic waste, such as cork, has gained considerable attention as a viable and sustainable adsorbent. Activated carbon is characterized by its high surface area, tunable porosity, and excellent adsorption capacity, making it highly effective for treating industrial effluents.[10] Producing activated carbon from cork stopper waste not only addresses the issue of waste reuse but also offers a low-cost and efficient alternative for the removal of organic pollutants.[11-13] Studies indicate that the porous structure of activated carbon, characterized by the ratio of micropores to mesopores, plays a crucial role in the adsorption of different types of pollutants, including industrial dyes.[14]

Activated carbon production is widely recognized as a well-established and consolidated process, applied in various industrial and environmental applications.[16] However, recent advances in its manufacturing have gained attention, with a focus on structural modifications and improvements that enable more precise control over its physicochemical properties. These developments include innovative synthesis methods that regulate pore formation, as well as surface functionalization to enhance its performance in specific applications, such as the removal of organic and inorganic pollutants from aqueous systems.[14,16-18]

Pore-structure control, with particular attention to the ratio between micropores, mesopores, and macropores, has become one of the most studied parameters due to its direct influence on the material's adsorption capacity.[19,20] Optimizing these features allows activated carbon to be tailored for adsorbing compounds of different molecular sizes, making it a versatile tool in environmental treatment. Recent studies have explored, for instance, physical and chemical activation techniques that promote controlled pore distribution, in addition to surface modifications that enhance interactions with specific contaminants such as heavy metals and industrial dyes.[21,22]

These collective efforts aim not only to enhance the efficiency of activated carbon but also to make it a more sustainable alternative by using lignocellulosic waste and other low-cost materials as precursors. In this context, the present study aims to synthesize activated carbon from cork stoppers using chemical activation with potassium hydroxide (KOH), characterize the physicochemical properties of the resulting material through Brunauer-Emmett-Teller (BET) surface area analysis, scanning electron microscopy (SEM), thermogravimetric analysis (TGA), Fourier transform infrared spectroscopy (FTIR), and X-ray diffraction (XRD), and evaluate its adsorption performance methylene blue (MB) and reactive red (RR) dyes in both batch and fixed-bed systems through kinetic, isotherm, and thermodynamic analyses.

2. Materials and methods

2.1. Ion of activated carbon

Cork stoppers, derived from wine and sparkling wine bottles, were used as the raw material in the present study. After collection, the stoppers were cleaned with running water to remove surface impurities and residual particles, then dried in an oven at 105°C for 24 h. Carbonization was carried out in a tubular furnace (Lindberg Blue M, Thermo Scientific) at 700°C with a heating rate of 10°C min^{-1} for 2 h under a continuous nitrogen flow (150 mL·min^{-1}). The resulting carbonized material was chemically activated using KOH pellets at a mass ratio of carbon: KOH = 4:1. Activation was carried out under similar conditions to carbonization, maintaining a heating rate of 10°C min^{-1} and a nitrogen atmosphere, at a final temperature of 850°C for 1.5 h. After activation, the material was washed

sequentially with 0.5 M hydrochloric acid (HCl) solution and warm distilled water (60°C) until a constant neutral pH was achieved. The cork-derived activated carbon (CAC) was then oven-dried at 105°C for 24 h.

2.2. Characterization

The material characterization procedures, including SEM, porosity analysis, TGA, FTIR, and XRD, followed the methods previously described by Domingos *et al.*[23] Briefly, the TGA and derivative thermogravimetric analyses of cork stoppers were performed using a TGA-50 analyzer (Shimadzu, Japan) under a nitrogen atmosphere (50 mL min^{-1}) at a heating rate of 10°C min^{-1} up to 900°C. Morphological characterization was carried out using SEM (JSM-6390LV, JEOL, Japan). FTIR spectra were recorded on an Agilent Cary 660 spectrometer (US), averaging 20 scans over the 4,000–500 cm^{-1} range, with a spectral resolution of 4 cm^{-1}. Crystalline phase identification was performed using XRD (Cad-4 diffractometer, Enraf-Nonius, Germany). Porosity and specific surface area were determined through physisorption using the Barrett–Joyner–Halenda and BET methods, respectively, with an Autosorb 1C analyzer (Quantachrome, US). The two-dimensional non-local density functional theory (DFT) heterogeneous surface model was applied to calculate pore size distribution, total pore volume (V_{total}), and specific surface area ($SSA_{DFT)}$ using the SAIEUS software (version 3.0, Micromeritics Instrument Corporation, USA). V_{total} was obtained from the cumulative pore size distribution, while the mesopore volume (V_{mes}) was determined by subtracting the micropore volume (V_{mic}) from V_{total}.

2.3. Batch adsorption

The adsorption performance of the CAC was evaluated using MB and RR PF-3B dyes. The effects of contact time, adsorbent dosage, dye concentration, temperature, and pH were systematically investigated.

In each batch experiment, 100 mL of dye solution was placed in Erlenmeyer flasks with a defined CAC dose and agitated in a thermostatic water-bath shaker (Marq Labor, BM/DR, Brazil). After adsorption, the supernatant was filtered and centrifuged at 10,000 rpm for 2 min. The residual dye concentration was determined using an ultraviolet-visible spectrophotometer at wavelengths of 665 nm (MB) and 538 nm (RR), based on corresponding calibration curves. Experiments were carried out under the following conditions: Agitation speed = 160 rpm; initial dye concentration = 50–250 mg/L; adsorbent dose = 0.2–1 g/L; pH = 3–11; and temperature = 25°C–55°C. The adsorption capacity (q_t, mg/g) and dye removal efficiency (R, %) were calculated using Equations (1) and (2), respectively:

$$q_t = \frac{C_0 - C_t}{m} \times V \quad (1)$$

$$R(\%) = \frac{C_0 - C_t}{C_0} \times 100 \quad (2)$$

Where C_0 (mg·L^{-1}) and C_t (mg·L^{-1}) are the dye concentrations at the initial time and time t, respectively; m (g) is the mass of CAC; and V (L) is the volume of the solution.

2.4. Adsorption models

The adsorption kinetics of the dyes were analyzed using the pseudo-first-order (PFO) model,[24] pseudo-second-order (PSO) model,[25] Elovich model,[26] and intraparticle diffusion model.[27] Adsorption isotherms were fitted using the Langmuir, Freundlich, and Redlich-Peterson models.[28] The kinetic and thermodynamic models applied in this study are detailed in Table S1.

2.5. Column adsorption

A fixed-bed column system was constructed to assess the continuous adsorption performance of the CAC for MB and RR (Figure 1). The adsorption column consisted of a cylindrical plexiglass tube (height = 10 cm; internal diameter = 1 cm). The column was packed with 1 g of CAC, and a layer of cotton and glass beads was placed at the top to prevent particle loss and clogging during operation. MB and RR dye solutions (100 mg/L) were continuously pumped upward at 25°C using a peristaltic pump at 32 mL/h. Effluent samples were collected at predetermined time intervals until column saturation was reached ($C/C_0 = 1$).

The breakthrough curve was obtained by plotting the ratio of the effluent concentration to the inlet concentration (C/C_0) as a function of time (t). The maximum dye adsorption capacity under specific flow, concentration, and bed height conditions was determined from the total area under the breakthrough curve, as described in Equation (3).

$$q_{total} = \frac{C_0 x F_m}{m_s} \int_{t=0}^{t=t_{total}} \frac{1 - C}{C_0} dt \quad (3)$$

Where q_{total} = maximum adsorption capacity in the column (mg g^{-1}); C_0 = initial dye concentration (mg L^{-1}); C = dye concentration at time t (mg L^{-1}); m_s = mass of the adsorbent (g); F_m = volumetric flow rate (L min^{-1}); t = time (min).

The performance of the system was further evaluated using the Thomas,[29] Clark (Hu *et al.*, 2000),[29] and Yoon-Nelson[30] models, whose kinetic expressions are presented in Table S1.

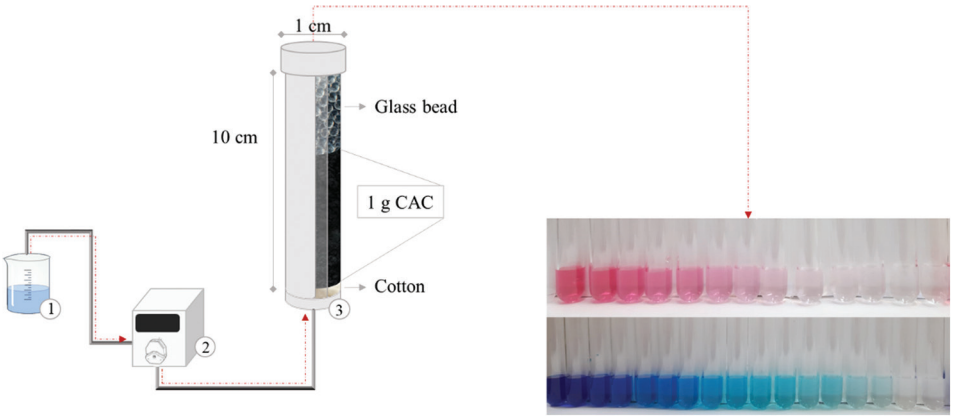

Figure 1. Schematic illustration of the adsorption column: (1) dye solution reservoir; (2) peristaltic pump; (3) adsorption column
Abbreviation: CAC: Cork-derived activated carbon.

3. Results and discussion

3.1. Adsorbent characterization

The characterization methods used in the present study were previously detailed by Domingos *et al.*,[30] where the same material was investigated. The data obtained in that work serve as a reference for understanding the present results, allowing for a direct correlation between studies of the material's properties.

Cork is widely recognized for its unique cellular structure, resembling a honeycomb, which provides high porosity and low density. These characteristics make it an excellent precursor for activated carbon production. Carbonization of cork at 700°C under a nitrogen atmosphere promotes the decomposition of organic components such as suberin, lignin, cellulose, and hemicellulose, resulting in an initial carbonaceous matrix. This process is evidenced by the TGA curves,[23] which show significant mass loss up to 450°C, with a total weight loss of approximately 75.2%. The greatest mass loss corresponds to the decomposition of lignin and suberin—the main constituents of cork—with 53.7% loss at 450°C.[31] Above 500°C, the rate of mass loss decreases, leaving approximately 3.79% of the original mass as ash.

Following carbonization, chemical activation with KOH at 850°C promotes the development of a highly porous structure (Table S2). KOH acts as a strong activating agent, inducing redox reactions between the activating agent and the carbon in the structure.[32] Initially, KOH reacts with carbon, forming intermediate compounds such as potassium carbonate (K_2CO_3) and potassium oxide (K_2O), along with gaseous products such as carbon monoxide and carbon dioxide (CO_2).[33]

Chemical activation with KOH is one of the most effective methods for producing activated carbons with high surface area and highly porous structures. Excess KOH and high temperatures promote continuous removal of carbon atoms, promoting the formation of micropores and mesopores. During the process, the decomposition of K_2CO_3 generates K_2O and releases CO_2, further enhancing pore development.[34] KOH thus acts both as an activating agent and as a chemical template, creating an interconnected microporous network that significantly increases surface area, often exceeding 1,500 m^2/g.[35] The activation temperature, especially around 850°C, plays a fundamental role in the structural modification of the material, resulting in a highly efficient adsorbent.[36] After activation with KOH, the activated carbon contains residual inorganic compounds, mainly K_2CO_3 and K_2O, which may obstruct micropores and compromise the material's adsorption efficiency. Washing with 0.5 M HCl dissolves these residues, forming soluble potassium chloride that is removed by subsequent rinsing with warm water. This acid treatment is essential to eliminate mineral impurities, preserve the porous structure formed during activation, and ensure accessibility of active adsorption sites.[37]

The BET and DFT analyses confirmed the high porosity of the CAC, demonstrating a balanced distribution between micropores and mesopores (Table 1). The specific surface area obtained by BET analysis (1,793 m^2/g) and confirmed by DFT (1,430 m^2/g) indicates the predominance of micropores (0.70 cm^3/g) with a notable contribution of mesopores (0.17 cm^3/g). These values indicate that the activated carbon is highly efficient for adsorbing both small and large organic molecules. The average pore diameter (1.33 nm) falls within the microporous range, reinforcing the microporous nature of the material.

The natural cellular structure of raw cork, composed of hollow polyhedral cells with thin walls, plays a crucial role in the development of porosity in the CAC (Figure 2A).

Table 1. Characteristics of CAC based on N_2 adsorption-desorption isotherms

Material	SSA_{BET} (m^2/g)	SSA_{DFT} (m^2/g)	V_{total} (cm^3/g)	V_{mic} (cm^3/g)	V_{mes} (cm^3/g)	$\%V_{mes}$	V_{mic}/V_{mes}	d_{50} (nm)
CAC	1,793	1,430	0.87	0.70	0.17	19	4.12	1.33

Abbreviations: CAC: Cork-derived activated carbon; d_{50}: Median pore diameter; SSA_{BET}: Specific surface area determined by the Brunauer-Emmett-Teller method; SSA_{DFT}: Specific surface area determined by the density functional theory model; V_{mes}: Mesopore volume; V_{mic}: Micropore volume; V_{total}: Total pore volume.

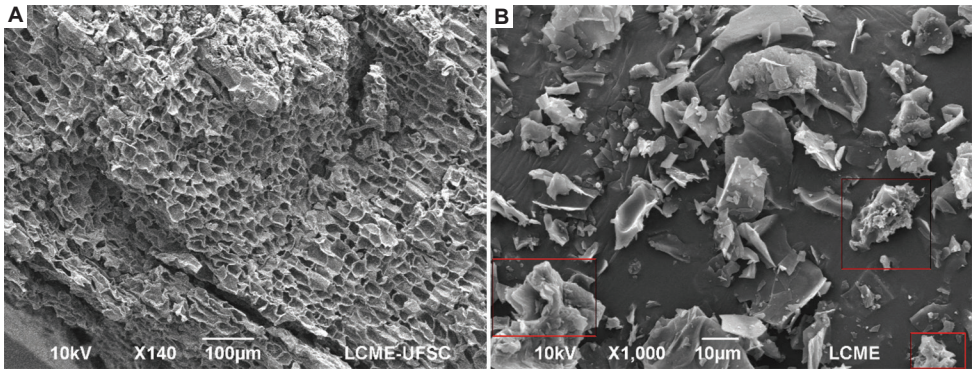

Figure 2. Scanning electron microscopy of cork stoppers and cork-derived activated carbon (CAC). (A) Structure of cork stopper. Scale bars: 100 µm; magnification: ×500. (B) Surface of CAC after activation. Scale bars: 10 µm; magnification: ×5,000.
Note: Red boxes indicate the regions selected for higher magnification imaging.

During carbonization and activation, these cells undergo significant structural transformations; however, part of their architecture is preserved (Figures 2B and S1), serving as a precursor for micropore and mesopore formation. The thin walls of cork cells decompose at high temperatures, generating an extensive network of micropores that results in a high surface area and excellent adsorption capacity for small molecules such as gases and volatile organic compounds[38] (Figure 2B). This behavior is reflected in the high V_{total} (0.87 cm^3/g), of which 0.70 cm^3/g corresponding to micropores.

The residual structure of cork's polyhedral cells also contributes to the structural integrity of the CAC, maintaining macropores that act as diffusion channels.[39] Although mesopores represent a smaller fraction of the V_{total} (0.17 cm^3/g), they play an essential role in transporting larger molecules, such as dyes and pesticides, toward the internal microporous regions where effective adsorption occurs.[40-42] During KOH activation, the process proceeds both radially and laterally: Radial activation generates micropores, while lateral activation expands them into mesopores, enhancing accessibility and enabling adsorption of molecules of varying sizes.[3]

The FTIR analysis of cork stoppers, as reported by Domingos *et al.*,[30] revealed functional groups characteristic of the main cork components, such as suberin, lignin, and cellulose, that persist after carbonization. The spectrum showed a peak at 3,437 cm^{-1}, associated with O–H stretching vibrations from hydroxyl (–OH) groups in alcohols, phenols, and adsorbed water typical of lignocellulosic materials. Peaks at 2,925 cm^{-1} and 2,854 cm^{-1} correspond to C–H stretching from long aliphatic chains of suberin, imparting hydrophobicity and stability. The peak at 1,738 cm^{-1} is attributed to carbonyl (C=O) stretching from suberin esters, reinforcing its structural role. Peaks at 1,626 cm^{-1} and 1511 cm^{-1} indicate the presence of conjugated C=O and C=C bonds related to lignin, which imparts rigidity to the material. Peaks at 1,462 cm^{-1} and 1,249 cm^{-1} correspond to C–H and C–O stretching in esterified fatty acids, while the signals at 1,159 cm^{-1} and 1,102 cm^{-1} are linked to C–O–C vibrations from polysaccharides such as cellulose and hemicellulose, which provide structural stability.[39]

After carbonization at 700°C and cork activation, chemical changes were observed in the material's structure, although some functional groups were preserved. The peak at 3,438 cm^{-1} confirms the presence of –OH groups that favor interaction with polar molecules such as dyes and metal ions. The peaks at 2,917 cm^{-1} and 2,852 cm^{-1} indicate the partial preservation of aliphatic chains from suberin, providing the material with hydrophobic properties and potential for adsorption of non-polar compounds. Signals at 1,109 cm^{-1} and 1,015 cm^{-1} suggest residual polysaccharides. In addition, the peak at 805 cm^{-1}, indicative of stable aromatic structures, suggests enhanced structural stability and adsorption potential for organic compounds.[12,43]

Activation with KOH is widely recognized for producing activated carbons with high porosity and significant microporosity.[44] However, this process also induces a disordered structure, as observed in the XRD pattern of CAC reported by Domingos *et al.*,[30] which exhibits a broad diffuse peak at 22° (2θ), indicative of a predominantly amorphous structure. This behavior is common in KOH-activated carbons, in which carbon removal hinders the formation of graphite crystalline layers, resulting in a disordered structural arrangement.[45] The absence of well-defined crystalline planes facilitates micropore formation and increases the surface area available for adsorption.[46,47] Furthermore, the absence of peaks around 43° (2θ), typically associated with organized graphitic planes, suggests that the CAC does not exhibit significant graphitization. Similar results were reported by Hardi *et al.*[48] for KOH-activated carbons derived from palm shells, reinforcing the trend that KOH activation promotes amorphous structures.

3.2. Batch adsorption using CAC

To evaluate the adsorption efficiency of CAC for MB and RR, the effects of variables such as contact time, pH, temperature, and initial dye concentration were investigated. Figure 3 illustrates the adsorption capacity of CAC as a function of time. CAC exhibited a higher affinity for MB, reaching approximately 250 mg/g (Figure 3A) within 5 min, while RR attained a maximum capacity of 105 mg/g (Figure 3D) after 75 min. This difference can be attributed to the smaller kinetic diameter of MB, which facilitates its diffusion into the micropores of the adsorbent. In contrast, RR experiences greater resistance due to its larger molecular size.[49-51] The molecular structure of reactive dyes directly influences their adsorption behavior. More complex compounds, such as RR, contain functional groups (e.g., sulfonate [$-SO_3^-$] and azo) and possess higher molecular weights, both of which hinder diffusion into the porous matrix of CAC, particularly in predominantly microporous materials.[52] In contrast,

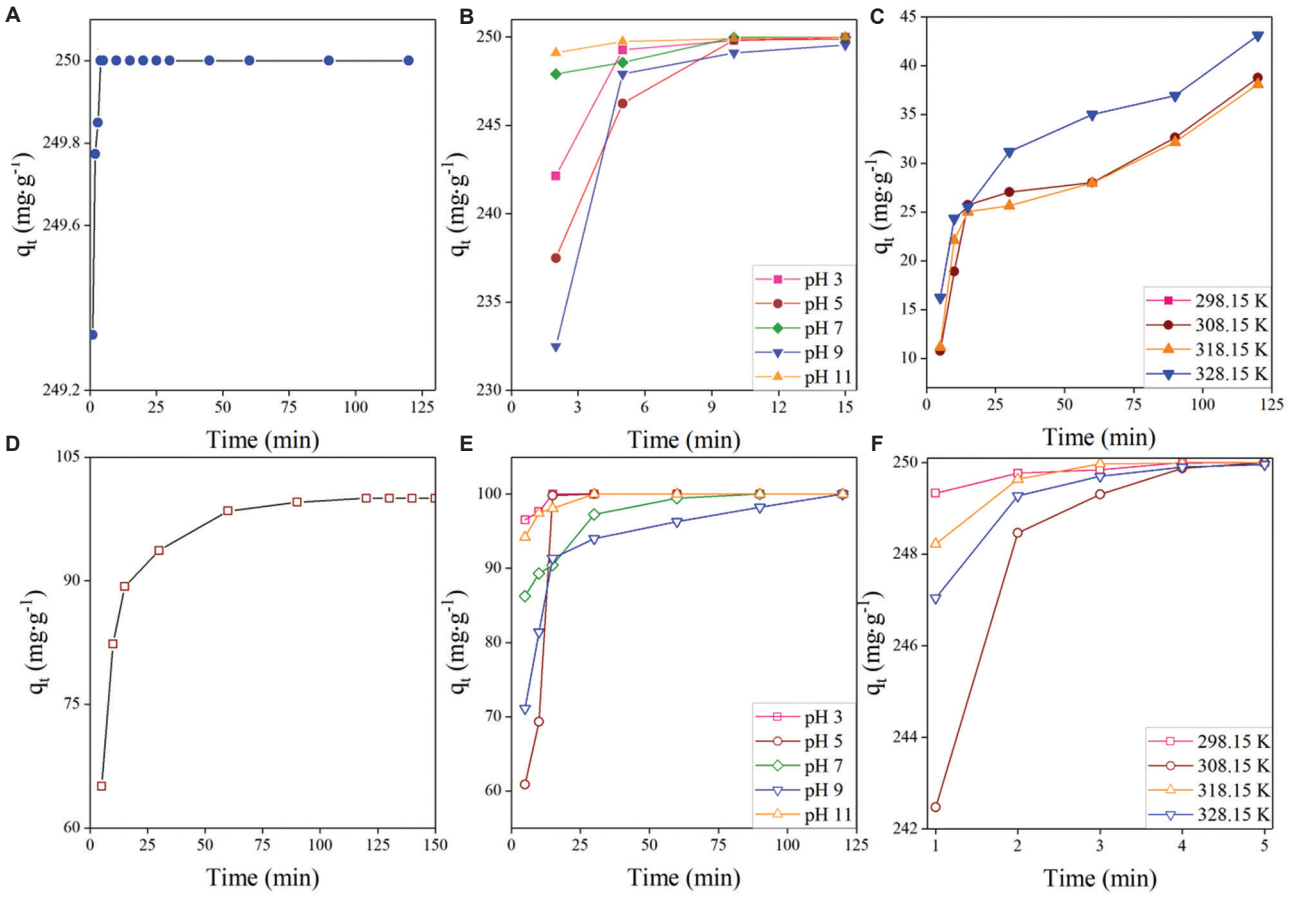

Figure 3. Adsorption kinetics of methylene blue (MB) and reactive red (RR) onto cork-derived activated carbon (CAC) under different experimental conditions. (A) Adsorption capacity over time for MB (C_0: 100 mg/L, T: 25°C, CAC: 0.4 g/L). (B) Effect of pH on MB adsorption kinetics (C_0: 100 mg/L, T: 25°C, CAC: 0.4 g/L). (C) Influence of temperature on MB adsorption (C_0: 100 mg/L, CAC: 0.4 g/L). (D) Adsorption capacity over time for RR (C_0: 100 mg/L, T: 25°C, CAC: 1 g/L). (E) Effect of pH on RR adsorption kinetics (C_0: 100 mg/L, T: 25°C, CAC: 1 g/L). (F) Influence of temperature on RR adsorption (C_0: 100 mg/L, CAC: 1 g/L).

smaller molecules such as MB reach adsorption equilibrium more efficiently due to lower diffusional resistance and weaker intermolecular interactions.[52,53]

The pH of the solution significantly affects both the surface charge of the adsorbent and the ionization state of the dye molecules. Wang *et al.*[54] reported that CAC produced using KOH exhibits a point of zero charge (pH_pzc) of approximately 2.2. At pH values above this threshold, the adsorbent surface becomes negatively charged, favoring adsorption of cationic species such as MB via electrostatic attraction. Accordingly, MB exhibited maximum uptake at alkaline pH conditions (pH 9–10), whereas RR, an anionic dye, was adsorbed more efficiently under acidic conditions (pH 3–4), where the positively charged CAC surface enhances electrostatic attraction (Figure 3B and E).

Temperature variations also impacted adsorption efficiency. For MB, higher temperatures (318–328 K) improved adsorption, consistent with an endothermic process driven by increased kinetic energy and enhanced molecular diffusion[54,55] (Figure 3C). In contrast, RR showed minimal thermal sensitivity (Figure 3F), suggesting that specific surface interactions play a more relevant role in its adsorption mechanism.

Based on the combined effects of contact time, pH, and temperature, optimal adsorption conditions were established for both dyes. For MB, the best performance was observed at alkaline pH (9–10), higher temperatures (44.85–55°C), and an adsorbent dose of 0.4 g/L, achieving a maximum capacity of approximately 250 mg/g within 5 min. For RR, optimal conditions were observed at acidic pH (3–4), room temperature (25°C), and an adsorbent dose of 1.0 g/L, achieving approximately 105 mg/g after 75 min.

3.3. Batch adsorption kinetics

3.3.1. Adsorption kinetics

Adsorption kinetics for MB and RR were analyzed using the PFO, PSO, Elovich, and intraparticle diffusion models, as illustrated in Figure 4 and detailed in Table S3. Kinetic

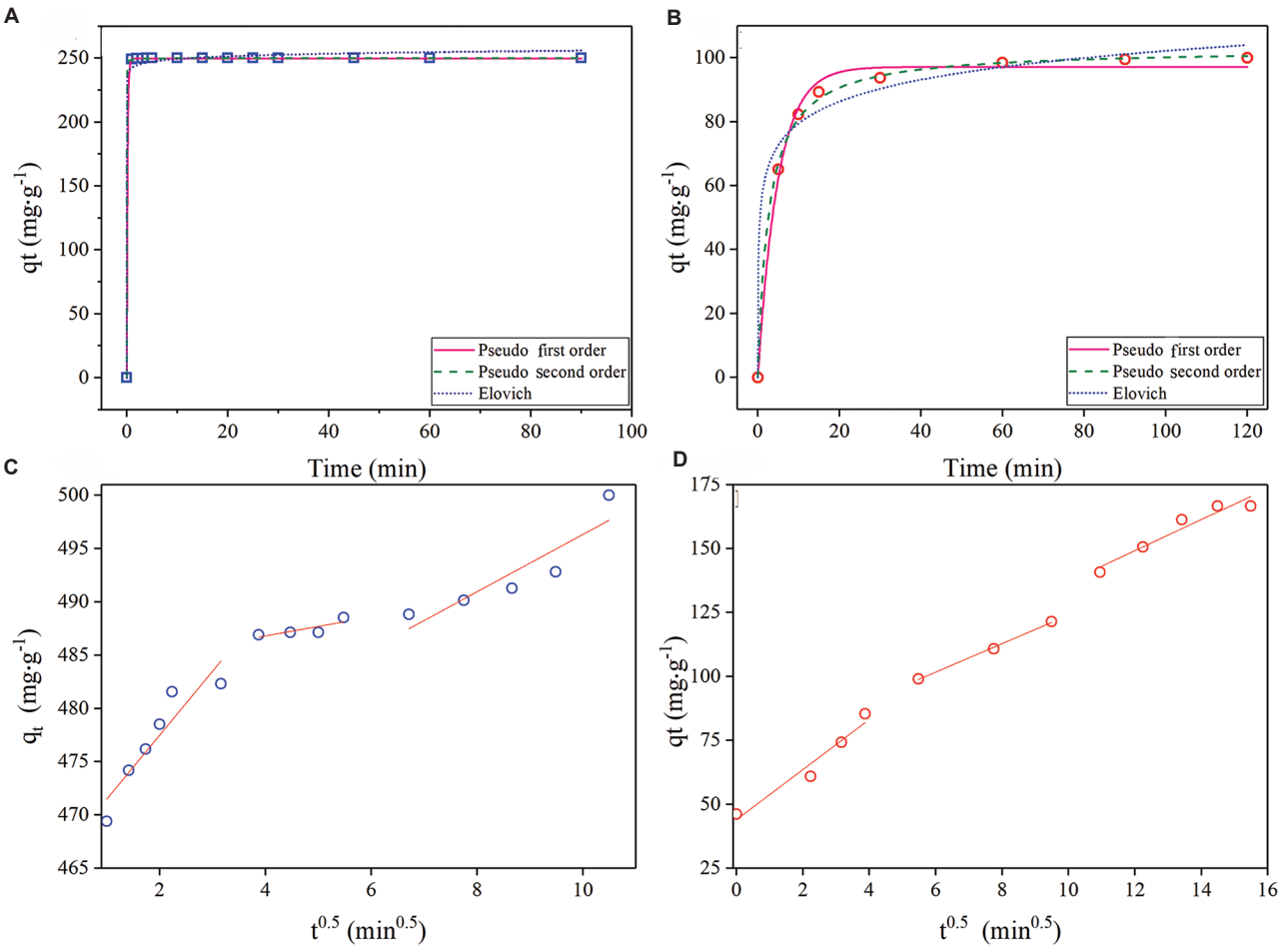

Figure 4. Kinetic modeling of dye adsorption fitted to pseudo-first-order, pseudo-second-order, and Elovich models for MB (A) and RR (B), and intraparticle diffusion analysis for MB (C) and RR (D)

modeling is essential for understanding the mechanisms governing adsorption, including the rate-limiting steps and the nature of interactions between adsorbent and adsorbate. By comparing the PFO, PSO, Elovich, and intraparticle diffusion models, it is possible to determine whether adsorption is governed by surface reactions, chemisorption, or diffusion processes. This approach also provides predictive parameters that are critical for scaling up adsorption systems from laboratory to industrial applications.[56] The experimental data showed the best fit with the PSO model, yielding determination coefficients (R^2) of 0.9985 for MB and 0.9987 for RR. These results suggest that the adsorption process is predominantly governed by chemical interactions between dye molecules and the functional groups present on the CAC surface.[57,58] Moreover, the Elovich model also described the data well, particularly for MB (R^2 = 0.9977), while RR demonstrated a good fit (R^2 = 0.9809), indicating that surface heterogeneity plays a significant role in the adsorption process.[59] To complement the kinetic interpretation, the intraparticle diffusion model was employed to evaluate the transport resistance of dyes within the porous structure of the CAC (Figure 4C and D). The results revealed three distinct adsorption phases: (i) an initial rapid phase, corresponding to external surface adsorption; (ii) an intermediate stage, representing gradual intraparticle diffusion; and (iii) a final equilibrium phase. The slope of the intermediate region suggests that intraparticle diffusion is not the sole rate-controlling step; other interactions, such as van der Waals forces, also influence the overall process.[60,61] For MB, the high microporosity of CAC (V_{mic} = 0.70 cm^3/g) facilitates rapid adsorption, whereas for RR, mesopores (Vmes = 0.17 cm^3/g) play a fundamental role in providing access to active sites.

3.3.2. Adsorption isotherms

Adsorption isotherm analyses for MB and RR were performed using the Langmuir, Freundlich, and Redlich-Peterson models, as presented in Figure 5 and Table S4. Isotherm modeling is critical for characterizing the adsorption process, including surface homogeneity, adsorbate–adsorbent affinity, and the potential for multilayer formation. These models also allow for the calculation of key parameters such as maximum adsorption capacity and adsorption intensity, which are essential for mechanistic interpretation and large-scale system design.[26] The isotherm analysis revealed distinct adsorption behaviors that reflect both the molecular characteristics of the dyes and the porosity of the adsorbent. The Langmuir model provided the best fit for MB, with an R^2 of 0.9857 (Figure 5A), indicating that adsorption predominantly occurs at homogeneous sites, consistent with the high microporosity of CAC. This monolayer adsorption behavior, likely governed by chemical interactions between MB and surface oxygenated groups, aligns with previous findings describing adsorption on homogeneous surfaces.[62,63] In contrast, the lower R^2 value (0.8454) of the Langmuir model for RR (Figure 5B) suggests that this model does not adequately capture the complexity of the interaction between RR and CAC. This limitation likely arises from the larger molecular size of RR and its reliance on mesopores for diffusion. The Freundlich model provided the best fit for RR (R^2 = 0.9998), indicating adsorption on energetically heterogeneous sites. This

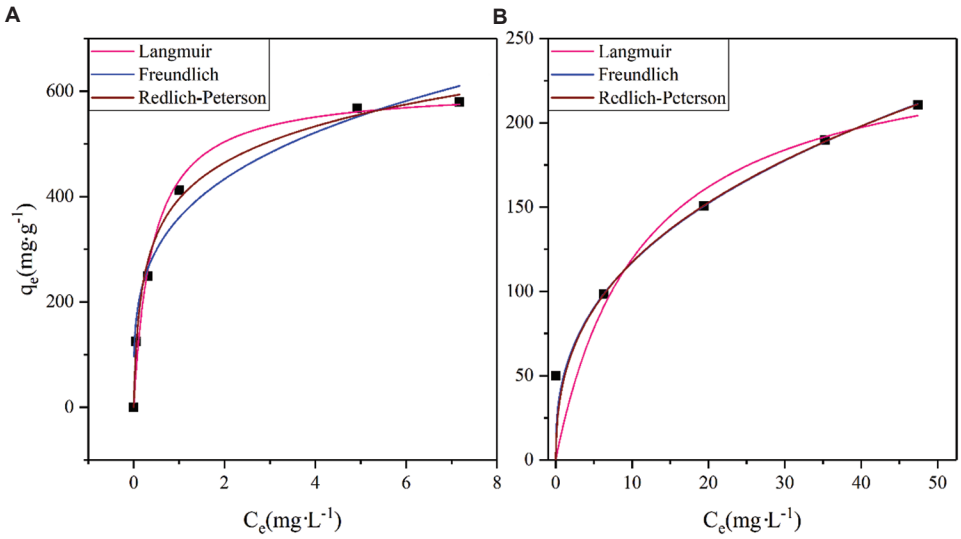

Figure 5. Adsorption isotherms fitted to the Langmuir, Freundlich, and Redlich–Peterson models for methylene blue (A) and reactive red (B) onto cork-derived activated carbon

model better captures the mesopore nature of CAC, which comprises 19% of the V_{total} (0.17 cm^3/g) and facilitates the transport of multilayer adsorption of larger RR molecules through van der Waals interactions. The Freundlich model thus effectively captures the heterogeneous distribution of adsorption sites on CAC and multilayer adsorption behavior.[43] The Redlich-Peterson model, which combines features of both the Langmuir and the Freundlich models, produced an excellent fit for MB (R^2 = 0.9941) with a parameter β = 0.84 (close to 1), suggesting that adsorption occurs primarily on a homogeneous surface, with only minor variations in adsorption energy not fully represented by the Langmuir model. However, for RR, the Redlich-Peterson model yielded a poorer fit (R^2 = 0.8562, β = 0.63), further supporting that the Freundlich model more accurately describes its adsorption on a heterogeneous surface.

Overall, the best-fitting models indicate that MB adsorption on CAC follows the Langmuir isotherm, implying monolayer adsorption at homogeneous sites, while RR adsorption is better described by the Freundlich isotherm, reflecting adsorption on heterogeneous sites and potential multilayer formation. This distinction arises from the larger molecular size and complex structure of RR, which require mesoporous access and promote non-uniform adsorption on heterogeneous surfaces.[64]

3.4. Adsorption thermodynamics

The evaluation of thermodynamic parameters for RR and MB adsorption provided a deeper understanding of the spontaneity and energetic nature of the process. As shown in Table S5, the negative values of Gibbs free energy indicate that both dyes are spontaneously adsorbed onto CAC at all analyzed temperatures. However, the energetic profiles of their interactions differ: While MB adsorption is endothermic, RR adsorption is exothermic, as evidenced by the negative enthalpy values (ΔH). The exothermic nature of RR adsorption suggests that the mechanism is predominantly governed by physical interactions, such as van der Waals forces and electrostatic attraction. As an anionic dye, RR contains $–SO_3^-$ groups that interact efficiently with the positively charged surface of activated carbon under acidic conditions (pH_pzc = 2.2). This electrostatic attraction between opposite charges promotes rapid but energetically weaker adsorption accompanied by heat release. Such behavior is typical of exothermic adsorption, in which the energy released during interaction is sufficient to stabilize the dye molecules on the surface without requiring additional activation energy.[65] The negative entropy variation (ΔS) for RR indicates a reduction in system disorder, suggesting that dye molecules are accommodated in a more ordered configuration on the adsorbent surface. This mechanism contrasts with MB adsorption, which occurs primarily within the micropores of activated carbon, facilitating π–π interactions and hydrogen bonding characteristics of an endothermic process in which elevated temperature favors the formation of stronger chemical bonds between the dye and the adsorbent surface.[66] The ΔH analysis reinforces this distinction. The endothermic nature of MB adsorption suggests stronger chemical interactions that require external energy input for stabilization. MB interacts with oxygenated surface groups on the activated carbon, forming chemical bonds and π–π interactions, which increase dye affinity as the temperature rises.[51] In contrast, RR adsorption exhibits negative ΔH values, confirming its exothermic nature and indicating that the process occurs without additional energy input. Because the predominant interactions are physical, the lower activation energy reflects a less selective mechanism in which the porous structure of the activated carbon plays a determining role. RR, being a larger molecule, faces higher diffusional resistance in micropores and is preferentially accommodated within the mesopores of the adsorbent, where interactions are less energetic.[67] ΔS further elucidates molecular organization during adsorption: Positive ΔS values for MB indicate an increase in system disorder associated with greater mobility of smaller molecules within the microporous network, whereas negative ΔS values for RR suggest more ordered adsorption, typical of bulky molecules fitting into mesopores in a structurally restrictive manner.[68]

3.4.1. Column adsorption

Figure 6 shows the breakthrough curve for MB and RR adsorption in a fixed-bed column packed with CAC. Initially, both dyes were efficiently removed, with the C_t/C_0 ratio remaining near zero until the breakthrough time (700–750 min), indicating high availability of active sites on CAC (Figure 6A). After 750 min, RR showed a sharp increase in outlet concentration ($C_t/C_0 > 0$), marking the breakthrough point and onset of the mass-transfer zone, signaling adsorbent saturation (Figure 6A). This behavior can be attributed to RR's higher molecular weight and anionic nature, which limit its access to CAC micropores and restrict intraparticle diffusion. In contrast, MB showed superior performance, with a breakthrough occurring around 800 min (Figure 6A). MB's smaller molecular size and cationic nature facilitate diffusion and promote electrostatic interactions with oxygenated surface groups on CAC, resulting in more prolonged dye removal.

The Clark and Yoon-Nelson models were applied to predict and interpret adsorption behavior in fixed-bed columns due to their ability to describe saturation dynamics and breakthrough in continuous systems

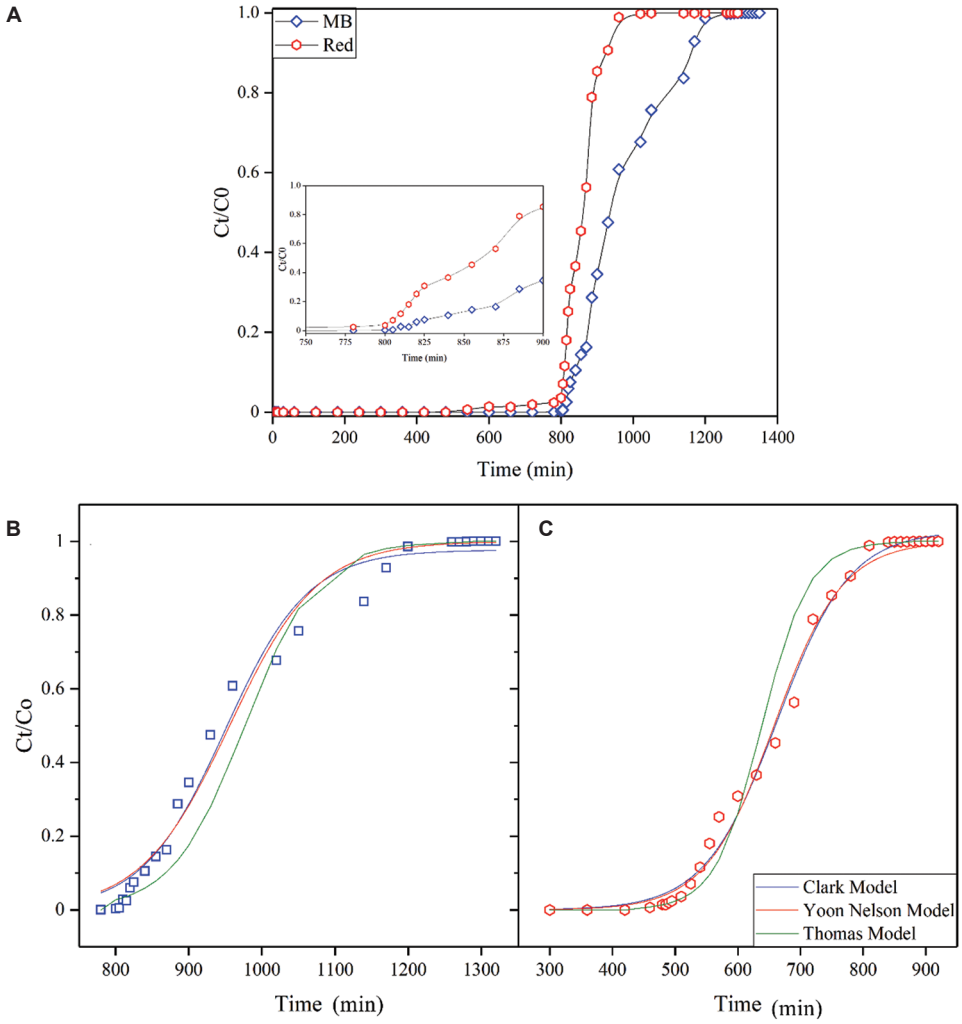

Figure 6. Breakthrough curves for methylene blue (MB) and reactive red (RR) adsorption onto cork-derived activated carbon in a fixed-bed column (A). The lines represent the fitting of the Clark, Yoon–Nelson, and Thomas models for MB (B) and RR (C).

(Figure 6B and C). Both models demonstrated excellent performance, with $R^2 > 0.9878$ for MB and RR (Table S6). Parameters derived from the Thomas model indicated that the adsorption rate constant was higher for MB (0.0083 mg/g) than for RR (0.0072 mg/g). The Clark model provided additional insights into total adsorption capacity (A) and saturation dynamics (Table S6). The parameter A was significantly higher for MB (1.9313×10^7 L/mg) than for RR (9.18145×10^4 L/mg). Despite these differences, the similarly low values of *r* (0.0176 for MB and 0.0172 for RR) suggest gradual saturation for both dyes, indicating a mechanism predominantly controlled by intraparticle transport. The Yoon–Nelson model further revealed that the rate constant (K_{YN}), which reflects the saturation rate, was higher for RR (0.0413 mg/g) than for MB (0.0328 mg/g), indicating that the column reached saturation more rapidly with RR. Conversely, the time required for 50% breakthrough (τ) was higher for MB (0.51 h) than for RR (0.44 h), demonstrating that MB provided greater operational stability before reaching 50% saturation. This inverse relationship between K_{YN} and τ reflects the balance between adsorption kinetics and total capacity, a behavior widely reported in continuous adsorption systems. These findings are also consistent with the Clark model results, which indicated a higher A for MB than for RR.

3.4.2. Adsorption mechanism

CAC demonstrated excellent properties for the adsorption of MB and RR. Its porous structure, characterized by a predominance of micropores (0.70 cm^3/g) and mesopores (0.17 cm^3/g), played a crucial role in the adsorption efficiency for both dyes. This balance between microporosity and mesoporosity provides CAC with significant versatility as an adsorbent, highlighting the

importance of a well-distributed pore structure for the efficient removal of contaminants with varying molecular sizes.[43,69] These results reinforce the relevance of the micropore-to-mesopore ratio (V_{mic}/V_{mes} = 4.12), which endows activated carbon with an optimal structure for efficiently adsorbing molecules of different sizes. Previous studies support this observation, demonstrating that the combination of micropores and mesopores plays a crucial role in optimizing dye adsorption. For example, Al-Degs *et al.*[65] emphasized that secondary micropore volumes, rather than total surface area, are key determinants of reactive dye adsorption. Similarly, Wu *et al.*[70] highlighted that micropores are essential for low-molecular-weight compounds, while mesopores facilitate the adsorption of larger molecules such as bulky dyes. Manocha and Brahmbhatt[71] showed that activated carbons with balanced proportions of micropores and mesopores exhibit higher adsorption capacities for MB, while Zhuang *et al.*[42] reported that ordered mesopores are essential for efficiently capturing bulky dyes in industrial effluents. These results are particularly relevant for materials with V_{mic}/V_{mes} ratios similar to the CAC evaluated in the present study. Furthermore, recent works by Abdoul *et al.*[40] and Subba Reddy *et al.*[72] revealed that increased mesoporosity not only enhances adsorption efficiency but also improves desorption rates, facilitating adsorbent regeneration. This characteristic is essential for industrial applications where material reuse is a priority. From a practical perspective, Table 2 summarizes the main aspects involved in the adsorption mechanisms of MB and RR.

In addition to pore distribution, the active sites of CAC play a central role in the adsorption mechanism. FTIR analysis confirmed the presence of oxygen-containing functional groups, such as –OH, carboxyl (–COOH), and C=O, which act as polar sites for hydrogen bonding and electrostatic interactions with dye molecules.[9] Graphitic domains on the carbon surface further contribute through π–π stacking with the aromatic rings of MB and RR.[54] The surface charge, defined by pH_pzc = 2.2, modulates the activity of these sites: At pH > pH_pzc, negatively charged sites ($–COO^-$) favor cationic dye adsorption (MB), while at pH < pH_pzc, protonated sites ($–OH_2^+$) enhance anionic dye adsorption (RR).[28] Together, these functional groups and charged sites form the main adsorption centers of CAC, working synergistically with its micro/mesoporous network to ensure high affinity toward structurally distinct molecules.

Table 2. Comparison of adsorption parameters for MB and RR onto CAC

Aspect	MB	RR
Type of adsorption	Chemisorption	Physisorption
Main porosity	Microporosity	Mesoporosity
Effect of pH	Optimized at high pH	Optimized at low pH
Effect of temperature	Endothermic (favored at high temperatures)	Exothermic (favored at low temperatures)
Kinetic model	PSO	PSO

Abbreviations: CAC: Cork-derived activated carbon; MB: Methylene blue; PSO: Pseudo-second-order; RR: Reactive red.

The high adsorption capacity of MB onto CAC results from a combination of electrostatic attraction, π–π interactions, and hydrogen bonding, along with a dynamic adaptation of the material's surface during adsorption.[66] At pH values above 2.2, CAC is negatively charged and exhibits a strong affinity toward cationic MB molecules, allowing adsorption equilibrium to be reached in <5 min. π–π interactions between the aromatic rings of MB and the conjugated domains of CAC promote close molecular association.[54] These interactions are supported by the characteristic C=C aromatic bond peaks in the FTIR spectrum (1,575 cm^{-1}), which remain intact after adsorption, indicating the structural stability of the activated carbon (Figure 7A).[10] MB retention is further reinforced by hydrogen bonds formed between –OH groups and possibly amine groups. The broadening of the peak at 3,419 cm^{-1} after adsorption indicates increased hydrogen-bonding intensity. This behavior is consistent with previous studies highlighting the crucial role of –OH groups in the adsorption of hydrophilic dyes.[73] The appearance of a new peak at 3,743 cm^{-1}, together with broadening at 3,419 cm^{-1}, suggests that adsorption-induced reorganization of functional groups on the CAC surface. This rearrangement, possibly involving –OH and other functional groups, reflects the material's ability to adapt its surface to optimize interactions with MB, promoting greater stabilization of the adsorbent-adsorbate complex.[10] FTIR spectra of the dyes are available in Figure S2 to complement the analysis of the observed interactions.

In contrast to MB, the adsorption of RR onto CAC occurs predominantly through physical interactions and is influenced by factors such as pH, porous structure, and temperature. Under strongly acidic pH conditions, the CAC surface becomes positively charged due to its pH_pzc = 2.2, favoring electrostatic interactions with $–SO_3^-$ of RR.[74] The adsorption of reactive dyes onto adsorbents depends heavily on specific forces such as electrostatic interactions, hydrogen bonding, and π–π interactions, whose efficiencies are directly affected by the dye's complex molecular architecture.[75] The performance of the adsorption process for such compounds requires tightly controlled conditions, including precise pH and temperature adjustments.[52,53] Van der Waals forces play

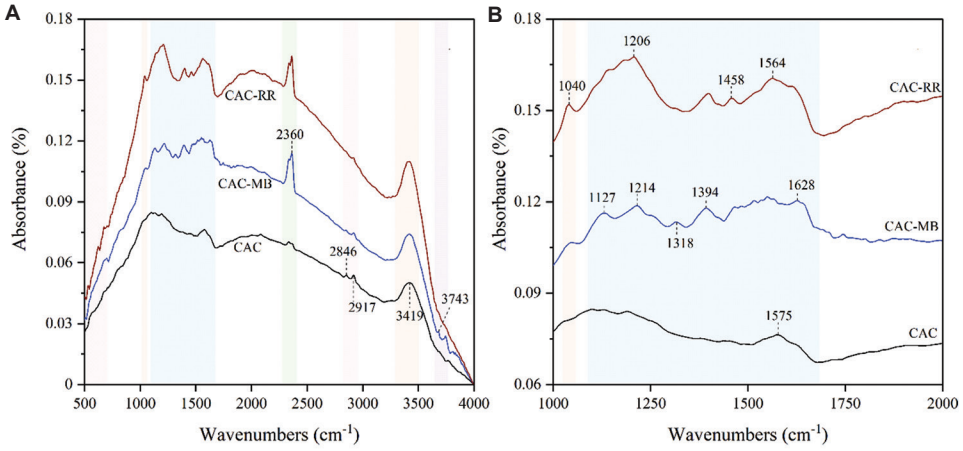

Figure 7. Fourier transforms infrared spectra of cork-derived activated carbon before and after dye adsorption (A), with a magnified view of the spectral region between 1,000 and 2,000 cm^{-1} (B)

a predominant role in this process, characterizing the physical adsorption (physisorption), as evidenced by the negative ΔH values, which indicate an exothermic reaction. This feature explains the reduced adsorption efficiency at elevated temperatures, as the weakening of interaction forces under thermal stress compromises dye retention.[76,77] The porous structure of CAC—with a balance between micropores and mesopores—is critical in this process. Mesopores facilitate the diffusion of larger molecules, while micropores contribute to efficient retention of the dye within internal active sites. However, an excessive predominance of micropores may limit adsorption efficiency due to diffusion barriers encountered by RR.[78] The FTIR peak at 3,419 cm^{-1} was broadened after adsorption, accompanied by the emergence of a new peak at 3,743 cm^{-1}, suggesting that –OH groups on the CAC surface actively participated in hydrogen bonding with the dye.[79] The $-SO_3^-$ groups of RR also played a key role, as indicated by intensified and shifted peaks in the 1,200–1,000 cm^{-1} region, attributed to S=O vibrations (Figure 7B). These changes indicate direct interactions between these groups and the active sites of CAC, reinforcing RR retention on the adsorbent surface.[80]

The adsorption mechanisms of MB and RR onto CAC involve both physical and chemical interactions; however, the dominant pathway differs for each dye. For MB, adsorption is mainly governed by chemisorption, as indicated by its strong fit to the PSO kinetic model, the Langmuir isotherm, and the endothermic nature of the process.[25,28] These results demonstrate strong interactions between MB molecules and negatively charged surface sites, reinforced by hydrogen bonding and π–π stacking.[54] In contrast, RR adsorption is predominantly physisorption. The process is exothermic, less stable at elevated temperatures, and better described by the Freundlich isotherm, reflecting heterogeneous adsorption sites and multilayer formation.[81] The bulky molecular structure of RR and the resulting steric hindrance limit its access to micropores, making mesopores essential for retention through weaker forces such as van der Waals interactions and intraparticle diffusion. Although hydrogen bonding also contributes, the overall mechanism is dominated by physisorption.

As summarized in Table S7, the adsorption capacity of CAC is comparable to or higher than that of several activated carbons reported in the literature. For instance, while almond shell- and rice husk-derived carbons exhibited adsorption capacities of 788 mg/g and 362.6 mg/g for MB, respectively, whereas CAC achieved 250 mg/g under optimized conditions, despite the higher molecular complexity of the dyes investigated. For RR, the capacity of 105 mg/g achieved by CAC significantly exceeds values reported for seaweed- and sewage-sludge-based carbons (33–132 mg/g), highlighting its efficiency toward bulky anionic dyes. These results demonstrate that cork, a lignocellulosic waste with unique structural features, is a highly competitive precursor for producing activated carbons that combine high adsorption performance with sustainability advantages.

4. Conclusion

This study demonstrated the potential of converting cork stopper waste into high-efficiency activated carbon for the removal of industrial dyes from aqueous matrices. Structural characterization revealed an optimized distribution of micropores and mesopores, resulting in a high specific surface area (1,793 m^2/g)—a key factor contributing to the material's adsorption efficiency. Under optimal conditions, the maximum adsorption capacities

reached 608 mg/g for MB and 252 mg/g for RR, with the differential efficiency attributed to structural and surface properties of the material. MB exhibited superior adsorption performance, driven by favorable electrostatic interactions under alkaline pH and its smaller molecular size, which facilitates diffusion into CAC's micropores. In contrast, RR adsorption was predominantly governed by physical interactions and intraparticle diffusion, highlighting the importance of mesopore distribution for retaining bulkier dyes. Kinetic modeling indicated that the adsorption process primarily followed the PSO model, suggesting the involvement of chemical interactions in MB adsorption, while RR was strongly affected by diffusion within the mesopores. The adsorption isotherms further supported this distinction: MB followed the Redlich-Peterson model, indicating adsorption on homogeneous surfaces, while RR followed the Freundlich model, consistent with heterogeneous adsorption sites. Thermodynamic parameters revealed that MB adsorption is an endothermic and spontaneous process favored at higher temperatures, while RR exhibited exothermic behavior and reduced efficiency at elevated temperatures. Fixed-bed column experiments confirmed the robustness of CAC in continuous systems, showing greater operational stability and adsorption capacity for MB, as evidenced by a longer breakthrough time compared to RR. The optimization of pore structure and favorable surface interactions of CAC support its potential for adsorption-based treatment of emerging contaminants, offering an effective and sustainable approach for wastewater treatment.

Acknowledgments

The authors gratefully acknowledge the support provided by LATEA – Laboratory of Environmental Technologies (Federal University of São Carlos), LABMAT – Department of Materials Engineering, and LABEFLU – Effluents Laboratory (both from the Federal University of Santa Catarina) for their technical assistance and access to research infrastructure essential to the development of this study.

Funding

This study was funded by the Brazilian National Council for Scientific and Technological Development (CNPq) through a doctoral scholarship (CNPq 142083/2019-4). The funders had no role in study design, data collection, analysis, or decision to publish.

Conflict of interest

The authors declare that they have no competing interests.

Author contributions

Conceptualization: Dayane G. Domingos, Luís A. M. Ruotolo, Maria Eliza Nagel-Hassemer
Formal analysis: Dayane G. Domingos, Marina C. de Moraes
Investigation: Dayane G. Domingos
Methodology: Dayane G. Domingos, Antonio I. Ramos Filho
Resources: Luís A. M. Ruotolo, Maria Eliza Nagel-Hassemer
Supervision: Luís A. M. Ruotolo, Maria Eliza Nagel-Hassemer
Validation: Luís A. M. Ruotolo, Maria Eliza Nagel-Hassemer
Writing–original draft: Dayane G. Domingos
Writing–review & editing: Beatriz Lima Santos Klienchen Dalari, Antonio I. Ramos Filho, Luís A. M. Ruotolo, Maria Ángeles Lobo-Recio, Maria Eliza Nagel-Hassemer

Ethics approval and consent to participate

The research complies with ethical standards, with the authors declaring no conflicts of interest. No tests were conducted on humans or animals.

Consent for publication

Not applicable.

Availability of data

All data generated or analyzed during this study are included in this published article. Additional information can be made available upon reasonable request to the corresponding author.

References

1. Yuan J, Lv Z, Aliyeva T, Chen X. Optimization of production, distribution, natural resources and capacity planning throughout process sector worldwide supply chains with various goals. *Resour Policy*. 2024;97:105187.

   doi: 10.1016/j.resourpol.2024.105187

2. Hameed J, Huo C, Albasher G, Abubakr M. Revisiting the nexus between financialization and natural Resource efficiency through the lens of financial development and green industrial optimization. *J Clean Prod.* 2024;468:143066.

   doi: 10.1016/j.jclepro.2024.143066

3. Luo F, Wang C, Luo S, Tong Q, Xu L. Optimizing natural resource markets : Accelerating green growth in the economic recovery. *Resour Policy*. 2024;89:104648.

   doi: 10.1016/j.resourpol.2024.104648

4. Azevedo J, Lopes P, Mateus N, de Freitas V. Cork, a natural choice to wine? *Foods*. 2022;11:2638.

   doi: 10.3390/foods11172638

5. Ramos A, Berzosa J, Clarens F, Marin M, Rouboa A. Environmental and socio-economic assessment of cork

waste gasification: Life cycle and cost analysis. *J Clean Prod.* 2020;249:119316.

doi: 10.1016/j.jclepro.2019.119316

6. Rives J, Fernandez-Rodriguez I, Rieradevall J, Gabarrell X. Environmental analysis of the production of natural cork stoppers in southern Europe (Catalonia e Spain). *J Clean Prod.* 2011;19:259-271.

doi: 10.1016/j.jclepro.2010.10.001

7. Demertzi M, Silva RP, Neto B, Dias AC, Arroja L. Cork stoppers supply chain: Potential scenarios for environmental impact reduction. *J Clean Prod.* 2016;112:1985-1994.

doi: 10.1016/j.jclepro.2015.02.072

8. Chander S, Lodha A, Veer K, Gupta A. Enhanced methylene blue dye sequestration by carbon-embedded mesoporous zinc oxide nanoparticles fabricated utilizing Aloe barbadensis miller biowaste: Batch optimization, simulation modeling, and textile effluent feasibility. *Mater Today Commun.* 2024;40:110107.

doi: 10.1016/j.mtcomm.2024.110107

9. Altowyan AS, Toghan A, Ahmed HA, *et al.* Removal of methylene blue dye from aqueous solution using carbon nanotubes decorated by nickel oxide nanoparticles via pulsed laser ablation method. *Radiat Phys Chem.* 2022;198:110268.

doi: 10.1016/j.radphyschem.2022.110268

10. Wang Q, Lai Z, Luo C, *et al.* Honeycomb-like activated carbon with microporous nanosheets structure prepared from waste biomass cork for highly efficient dye wastewater treatment. *J Hazard Mater*. 2021;416:125896.

doi: 10.1016/j.jhazmat.2021.125896

11. Mallek M, Chtourou M, Portillo M, *et al.* Granulated cork as biosorbent for the removal of phenol derivatives and emerging contaminants. *J Environ Manage*. 2018;223:576-585.

doi: 10.1016/j.jenvman.2018.06.069

12. Mestre AS, Pires RA, Aroso IM, *et al.* Activated carbons prepared from industrial pre-treated cork: Sustainable adsorbents for pharmaceutical compounds removal. *Chem Eng J.* 2014;253:408-417.

13. Pintor AMA, Ferreira CIA, Pereira JC, *et al.* Use of cork powder and granules for the adsorption of pollutants : A review. *Water Res*. 2012;46:3152-3126.

doi: 10.1016/j.watres.2012.03.048

14. Novais RM, Caetano APF, Seabra MP, Labrincha JA, Pullar RC. Extremely fast and efficient methylene blue adsorption using eco-friendly cork and paper waste-based activated carbon adsorbents. *J Clean Prod.* 2018;197:1137-1147.

15. Giles MA, Danell R. Water dechlorination by activated carbon, ultraviolet radiation and sodium for fish culture. *Water Res*. 1983;17:667-676.

doi: 10.1016/0043-1354(83)90236-1

16. Chen Y, Tang Q, Shen C, Lei Y, Chen X. Activation-self-activation strategy for one-step preparation of Platycladus orientalis leaves based N-O-S self-doping hierarchical porous carbon for high-performance supercapacitor. *Ind Crops Prod.* 2025;225:120584.

doi: 10.1016/j.indcrop.2025.120584

17. Xu J, Guo M, Lin M, Ma C, Chen G. Three-dimensional nitrogen-doped modified activated carbon/graphene composite aerogel for highly efficient removal of indoor formaldehyde. *J Environ Chem Eng.* 2025;13:115576.

doi: 10.1016/j.jece.2025.115576

18. Quan C, Miskolczi N, Feng S, Grammelis P, Wu C, Gao N. Effect of type of activating agent on properties of activated carbon prepared from digested solid waste. *J Environ Manage*. 2023;348:119234.

doi: 10.1016/j.jenvman.2023.119234

19. Zhao Z, Wu W, Li W, *et al.* Adsorption recovery of chlorinated volatile organic compounds on coffee ground-based activated carbon of tunable porosity. *Sep Purif Technol.* 2025;354:129271.

doi: 10.1016/j.seppur.2024.129271

20. Zou Q. Corn-straw-converted activated carbons with tunable porosity and N/O functionalities as high-performance supercapacitors electrode at commercial-level mass loading. *J Energy Storage*. 2023;72:108673.

doi: 10.1016/j.est.2023.108673

21. Zhang Z, Liu X, Li D, *et al.* Mechanism of ultrasonic impregnation on porosity of activated carbons in non-cavitation and cavitation regimes. *Ultrason Sonochem*. 2019;51:206-213.

doi: 10.1016/j.ultsonch.2018.10.024

22. Guo Z, Zhang A, Zhang J, Liu H, Kang Y, Zhang C. An ammoniation-activation method to prepare activated carbon with enhanced porosity and functionality. *Powder Technol*. 2017;309:74-78.

doi: 10.1016/j.powtec.2016.12.068

23. Domingos DG, Barcelos KM, Oliveira KSGC, Juchen PT, Ruotolo LAM, Hassemer MEN. Cork activated carbon as a new sustainable electrode for electrochemical desalination: Customized surface chemistry for improved performance. *Electrochim Acta*. 2024;507:145120.

doi: 10.1016/j.electacta.2024.145120

24. Lagergren S. About the theory of so-called adsorption of soluble substances. In: *Kungliga Svenska Vetenskapsakademiens Handlingar*; 1898. p. 1-39.

25. Ho YS, Mckay G. Sorption of dye from aqueous solution by peat. *Chem Eng J.* 1998;70:115-124.

26. Ferreira AS, Mota AA, Oliveira AM, *et al.* Equilibrium and kinetic modelling of adsorption: Evaluating the performance of adsorbent in softening water for irrigation and animal consumption. *Rev Virtual Quim*. 2019;11:1752-1766.

27. Weber WJ, Morris JC. Kinetics of adsorption on carbon from solution. *J Sanit Eng Div.* 1963;89:31-60.

28. Ayawei N, Ebelegi AN, Wankasi D. Modelling and interpretation of adsorption isotherms. *J Chem.* 2017;2017:3039817.

doi: 10.1155/2017/3039817

29. Chen S, Yue Q, Gao B, Li Q, Xu X, Fu K. Bioresource Technology Adsorption of hexavalent chromium from aqueous solution by modified corn stalk : A fixed-bed column study. *Bioresour Technol.* 2012;113:114-120.

doi: 10.1016/j.biortech.2011.11.110

30. Omitola OB, Abonyi MN, Akpomie KG, Dawodu FA. AdamsBohart, YoonNelson, and Thomas modeling of the fixbed continuous column adsorption of amoxicillin onto silver nanoparticle - maize leaf composite. *Appl Water Sci.* 2022;12:94.

31. Silva SP, Sabino MA, Fernandes EM, Correlo VM, Boesel LF, Reis RL. Cork: Properties, capabilities and applications. *Int Mater Rev.* 2013;50:345-363.

32. Guo J, Lua AC. Textural and chemical characterizations of adsorbent prepared from palm shell by potassium hydroxide impregnation at different stages. *J Colloid Interface Sci*. 2002;233:227-233.

doi: 10.1006/jcis.2002.8587

33. Zornitta RL, Srimuk P, Lee J, *et al.* Charge and potential balancing for optimized capacitive deionization using lignin-derived, low-cost activated carbon electrodes. *ChemSusChem*. 2018;11:2101-2113.

doi: 10.1002/cssc.201800689

34. Bagheri N, Abedi J. Chemical Engineering Research and Design Preparation of high surface area activated carbon from corn by chemical activation using potassium hydroxide. *Chem Eng Res Des*. 2009;7:1059-1064.

doi: 10.1016/j.cherd.2009.02.001

35. Singh G, Maria Ruban A, Geng X, Vinu A. Recognizing the potential of K-salts, apart from KOH, for generating porous carbons using chemical activation. *Chem Eng J*. 2023;451:139045.

doi: 10.1016/j.cej.2022.139045

36. Luo J, Jiang T, Li G, Peng Z, Rao M, Zhang Y. Porous materials from thermally activated kaolinite: Preparation, characterization and application. *Materials (Basel).* 2017;10:647.

doi: 10.3390/ma10060647

37. Williams NE, Oba OA, Aydinlik NP. Modification, production, and methods of KOH-activated carbon. *ChemBioEng Rev*. 2022;9:164-189.

doi: 10.1002/cben.202100030

38. Xu X, *et al.* Natural Honeycomb-like structure cork carbon with hierarchical Micro-Mesopores and N-containing functional groups for VOCs adsorption. *Appl Surf Sci.* 2021;565:150550.

doi: 10.1016/j.apsusc.2021.150550

39. Cardoso B, Mestre AS, Carvalho AP, Pires J. Activated carbon derived from cork powder waste by KOH activation: Preparation, characterization, and VOCs adsorption. *Ind Eng Chem Res.* 2008;47:5841-5846.

40. Abdoul HJ, Yi M, Prieto M, *et al.* Efficient adsorption of bulky reactive dyes from water using sustainably-derived mesoporous carbons. *Environ Res.* 2023;221:115254.

doi: 10.1016/j.envres.2023.115254

41. Yuan X, Zhuo SP, Xing W, *et al.* Aqueous dye adsorption on ordered mesoporous carbons. *colloid Interface Sci.* 2007;310:83-89.

doi: 10.1016/j.jcis.2007.01.069

42. Zhuang X, Wan Y, Feng C, Shen Y, Zhao D. Highly efficient adsorption of bulky dye molecules in wastewater on ordered mesoporous carbons. *Chem Mater.* 2009;21:706-716.

doi: 10.1021/cm8028577

43. Wang Q, He D, Li C, Sun Z, Mu J. Honeycomb-like cork activated carbon modified with carbon dots for high-efficient adsorption of Pb(*II*) and rhodamine B. *Ind Crops Prod.* 2023;196:116485.

doi: 10.1016/j.indcrop.2023.116485

44. Feng S, Ouyang Q, Huang J, *et al.* Conversion of lignin into porous carbons for high-performance supercapacitors via spray drying and KOH activation: Structure-properties relationship and reaction mechanism. *J Renew Mater.* 2024;12:1207-1218.

doi: 10.32604/jrm.2024.052579

45. Apriyani I, Farma R, Awitdrus A, Yunita A. The amorphous porous carbon incorporating 1D-nanofiber as electroactive biomass with integrated pyrolysis for high-performance symmetrical supercapacitors. *Inorg Chem Commun.* 2024;169:113069.

doi: 10.1016/j.inoche.2024.113069

46. Sinaga DS, Indayaningsih N. Synthesis of conductive carbon sheet from coconut fiber with the addition of potassium hydroxide (KOH) activator. *J Technomater Phys.* 2022;4:63-67.

doi: 10.32734/jotp.v4i1.8177

47. Anas M, Jahiding M, Sudiana IN. Production and characterization of activated carbon from cashew nut shell using N2 as activation agent. *IOP Conf Ser Mater Sci Eng.*

2019;550:012035.

48. Hardi AD, Joni R, Syukri S, & Aziz, H. Production of Activated Carbon from Empty Palm Fruit Bunches as Supercapacitor Electrodes. Unand Physics J. 2021;9(4):479-486.

doi: 10.25077/jfu.9.4.479-486.2020

49. Aguiar JE, de Oliveira JCA, Silvino PFG, Neto JA, Silva IJ Jr., Lucena SMP. Correlation between PSD and adsorption of anionic dyes with different molecular weigths on activated carbon. *Colloids Surf A Physicochem Eng Asp.* 2016;496:125-131.

50. Hadi P, Yeung KY, Barford J, An KJ, McKay G. Significance of 'effective' surface area of activated carbons on elucidating the adsorption mechanism of large dye molecules. *J Environ Chem Eng*. 2015;3:1029-1037.

doi: 10.1016/j.jece.2015.03.005

51. Streit AFM, Pereira HA, Moreno-Pérez J, *et al.* New study of the adsorption mechanism of different dye molecules by high porous sludge activated carbon produced from a dairy-treatment effluent plant. *J Environ Chem Eng*. 2024;12:113745.

doi: 10.1016/j.jece.2024.113745

52. Langhals H, Sprenger S, and Brandherm MT. Perylenamidine-imide dyes. Liebigs Annalen. 1995:481-486.

doi: 10.1002/jlac.199519950366

53. Li B, Dong Y, Ding Z, Xu Y, Zou C. Renovation and reuse of reactive dyeing effluent by a novel heterogeneous fenton system based on metal modified PTFE fibrous catalyst/ H_2O_2. *Int J Photoenergy*. 2013;2013:169493.

54. Wang Q, Luo C, Lai Z, Chen S, He D, Mu J. Honeycomb-like cork activated carbon with ultra-high adsorption capacity for anionic, cationic and mixed dye: Preparation, performance and mechanism. *Bioresour Technol.* 2022;357:127363.

doi: 10.1016/j.biortech.2022.127363

55. Saeed A, Sharif M, Iqbal M. Application potential of grapefruit peel as dye sorbent : Kinetics, equilibrium and mechanism of crystal violet adsorption. *J Hazard Mater.* 2010;179:564-572.

doi: 10.1016/j.jhazmat.2010.03.041

56. Mohamed Nasser S, Abbas M, Trari M. Understanding the rate-limiting step adsorption kinetics onto biomaterials for mechanism adsorption control. *Prog React Kinet Mech.* 2024;49:1-26.

doi: 10.1177/14686783241226858

57. Pereira MFR, Soares SF, Órfão JJM, Figueiredo JL. Adsorption of dyes on activated carbons: Influence of surface chemical groups. *Carbon*. 2003;41:811-821.

doi: 10.1016/S0008-6223(02)00406-2

58. Pego MFF, Bianchi ML, Carvalho JA, Veiga TRLA. Surface modification of activated carbon by corona treatment. *An Acad Bras Cienc*. 2019;91:e20170947.

doi: 10.1590/0001-3765201920170947

59. Farias JP, Demarco CF, Afonso TF, *et al.* Comparison of the adsorption kinetics of methylene blue using rice husk ash activated with different chemical agents. *Rev Bras Ciên Ambient*. 2022;57:279-289.

doi: 10.5327/Z2176-94781195

60. Dharmarathna SP, Priyantha N. Investigation of boundary layer effect of intra-particle diffusion on methylene blue adsorption on activated carbon. *Energy Nexus*. 2024;14:100294.

doi: 10.1016/j.nexus.2024.100294

61. Valderrama C, Gamisans X, de las Heras X, Farrán A, Cortina JL. Sorption kinetics of polycyclic aromatic hydrocarbons removal using granular activated carbon: Intraparticle diffusion coefficients. *J Hazard Mater.* 2008;157:386-396.

doi: 10.1016/j.jhazmat.2007.12.119

62. Dhaouadi F, Sellaoui L, Dotto GL, Bonilla-Petriciolet A, Erto A, Lamine AB. Adsorption of methylene blue on comminuted raw avocado seeds : Interpretation of the effect of salts via physical monolayer model. *J Mol Liq J.* 2020;305:112815.

doi: 10.1016/j.molliq.2020.112815

63. Ghaffar A, Younis MN. Interaction and thermodynamics of methylene blue adsorption on oxidized multi-walled carbon nanotubes. *Green Process Synth*. 2015;4:209-217.

doi: 10.1515/gps-2015-0009

64. Belhachemi M, Addoun F. Comparative adsorption isotherms and modeling of methylene blue onto activated carbons. *Appl Water Sci*. 2011;1:111-117.

65. Al-Degs YS, El-Barghouthi MI, Khraisheh MA, Ahmad MN, Allen SJ. Effect of surface area, micropores, secondary micropores, and mesopores volumes of activated carbons on reactive dyes adsorption from solution. *Sep Sci Technol.* 2005;39:97-111.

66. Tran HN, Wang YF, You SJ, Chao HP. Insights into the mechanism of cationic dye adsorption on activated charcoal: The importance of Π–Π interactions. *Process Saf Environ Prot.* 2017;107:168-180.

doi: 10.1016/j.psep.2017.02.010

67. Wang Y, Chen Y, Zhao H, *et al.* Biomass-derived porous carbon with a good balance between high specific surface area and mesopore volume for supercapacitors. *Nanomaterials (Basel)*. 2022;12:3804.

doi: 10.3390/nano12213804

68. Sellaoui L, Lima EC, Dotto GL, Lamine AB. Adsorption of

amoxicillin and paracetamol on modified activated carbons: Equilibrium and positional entropy studies. *J Mol Liq.* 2017;234:375-381.

doi: 10.1016/j.molliq.2017.03.111

69. Liu X, Zhu H, Gong L, Jiang L, Lin D, Yang K. New insights into hierarchical pore size and level of concentration in efficient removal of toluene vapor by activated carbon. *Sci Total Environ.* 2022;853:158719.

doi: 10.1016/j.scitotenv.2022.158719

70. Wu FC, Tseng RL, Hu CC. Comparisons of pore properties and adsorption performance of KOH-activated and steam-activated carbons. *Microporous Mesoporous Mater.* 2005;80:95-106.

doi: 10.1016/j.micromeso.2004.12.005

71. Manocha S, Brahmbhatt A. Development of microporous activated carbon using a polymer blend technique and its behavior towards methylene blue adsorption. *Carbon Lett.* 2011;12:85-89.

doi: 10.5714/CL.2011.12.2.085

72. Subba Reddy Y, Rotte NK, Hussain S, Srikanth VVSS, Chandra MR. Sustainable mesoporous graphitic activated carbon as biosorbent for efficient adsorption of acidic and basic dyes from wastewater: Equilibrium, kinetics and thermodynamic studies. *J Hazard Mater Adv.* 2023;9:100214.

doi: 10.1016/j.hazadv.2022.100214

73. Olivella MÀ, Fiol N, de la Torre F, Poch J, Villaescusa I. A mechanistic approach to methylene blue sorption on two vegetable wastes: Cork bark and grape stalks. *BioResources.* 2012;7:3340-3354.

doi: 10.15376/biores.7.3.3340-3354

74. Nascimento VX, Pinto D, Lütke SF, *et al.* Brilliant blue FCF dye adsorption using magnetic activated carbon from Sapelli wood sawdust. *Environ Sci Pollut Res.* 2023;30:58684-58696.

doi: 10.1007/s11356-023-26646-6

75. El-Desouky MG, Khalil MAG, El-Afify MAM, El-Bindary AA, El-Bindary MA. Effective methods for removing different types of dyes-modelling analysis, statistical physics treatment and DFT calculations : A review. *Desalination Water Treat.* 2022;280:89-127.

doi: 10.5004/dwt.2022.29029

76. Aragaw TA, Alene AN. A comparative study of acidic, basic, and reactive dyes adsorption from aqueous solution onto kaolin adsorbent: Effect of operating parameters, isotherms, kinetics, and thermodynamics. *Emerg Contam.* 2022;8:59-74.

doi: 10.1016/j.emcon.2022.01.002

77. Behloul H, Ferkous H, Bougdah N, *et al.* New insights on the adsorption of CI-Reactive Red 141 dye using activated carbon prepared from the ZnCl2-treated waste cotton fibers: Statistical physics, DFT, COSMO-RS, and AIM studies. *J Mol Liq.* 2022;364:119956.

doi: 10.1016/j.molliq.2022.119956

78. Khraisheh MAM, Al-Degs YS, Allen SJ, Ahmad MN. Elucidation of controlling steps of reactive dye adsorption on activated carbon. *Ind Eng Chem Res.* 2002;41:1651-1657.

doi: 10.1021/ie000942c

79. Lafi R, Montasser I, Hafiane A. Adsorption of congo red dye from aqueous solutions by prepared activated carbon with oxygen-containing functional groups and its regeneration. *Adsorpt Sci Technol.* 2019;37:160-181.

80. Altaleb HA. Effective removal of hazardous cationic dye from polluted water using sulfonated copolymer hydrogel : Synthesis, nonlinear isotherm, and kinetics investigation. *J Saudi Chem Soc.* 2024;28:101852.

81. Foo KY, Hameed BH. Utilization of rice husks as a feedstock for preparation of activated carbon by microwave induced KOH and K2CO3 activation. *Bioresour Technol.* 2011;102:9814-9817.

doi: 10.1016/j.biortech.2011.07.102